Dual-Bridge LLC Resonant Converter With Fixed-Frequency PWM Control for Wide Input Applications

Xiaofeng Sun, *Member, IEEE*, Xiaohua Li, Yanfeng Shen, *Student Member, IEEE*, Baocheng Wang, and Xiaoqiang Guo, *Senior Member, IEEE*

***Abstract*—This paper proposes a dual-bridge (DB) LLC resonant converter for wide input applications. The topology is an integration of a half-bridge (HB) LLC circuit and a full-bridge (FB) LLC circuit. The fixed-frequency pulsewidth-modulated (PWM) control is employed and a range of twice the minimum input voltage can be covered. Compared with the traditional pulse frequency modulation (PFM) controlled HB/FB LLC resonant converter, the voltage gain range is independent of the quality factor, and the magnetizing inductor has little influence on the voltage gain, which can simplify the parameter selection process and benefit the design of magnetic components as well. Over the full load range, zero-voltage switching (ZVS) and zero-current switching (ZCS) can be achieved for primary switches and secondary rectifier diodes, respectively. Detailed analysis on the modulation schedule and operating principle of the proposed converter is presented along with the converter performance. Finally, all theoretical analysis and characteristics are verified by experimental results from a 120-V to 240-V input 24 V/20 A output converter prototype.**

***Index Terms*—Dual bridge (DB), fixed frequency, LLC, wide input voltage range.**

I. Introduction

In many applications, power conversion circuits are required to operate with a wide input-voltage range. For example, the output-voltage range of plug-in and battery electric vehicle (EV) on-board chargers is wide (e.g., 200–450 V), which means the input-voltage range of on-board dc/dc converters that condition power between the high- and low-voltage batteries is wide as well [1]–[4]. Therefore, developing a dc/dc converter with high efficiency over a wide voltage range is necessary.

LLC resonant converter, which is capable of realizing soft switching from zero to full loads and achieving high efficiency and high power density, has become a research hotspot in recent years [5]–[12]. Normally, conventional half- and full-bridge LLC converters work with variable frequency control. The operating frequency range has to be extended or the inductor ratio has to be decreased in order to obtain a wide input voltage range [13], [14], which is very challenging to design and optimize magnetic components [15]. This may cause many undesired problems such as low power density and high conduction losses. Therefore, the conventional LLC converter is not suitable for wide input applications [14].

Combining the three-level circuit with an LLC resonant tank, many types of three-level LLC (TL LLC) resonant converters capable of achieving a wide input range have been proposed in [16]–[21]. A simple TL LLC resonant dc/dc converter with only one magnetic component is proposed in [16], which can achieve a wide input/output range within a narrow frequency range because of the two-stage resonance. Different from the TL LLC resonant converters with one resonant tank, the topology discussed in [17] is a TL LLC resonant converter consisting of two half-bridge (HB) LLC series resonant converters in series, but sharing the same resonant inductor and transformer. As an extension of [17], another TL LLC converter with one resonant tank is proposed in [18], where the resonant frequency is twice as high as the switching frequency, decreasing the size of resonant components and increasing the power density. However, the frequency variations of these aforementioned converters are still relatively large, e.g., 88–150 kHz in [16], which is challenging for the optimization of magnetic components. By using the new modulation strategies, a TL isolated FB LLC converter that can operate at a fixed frequency is presented in [19], which can operate in entire two-level or three-level modes depending on the voltage range. However, a number of switches have to be employed and the structure is complex. Jin and Ruan [20] proposed a hybrid FB TL LLC converter capable of operating under both three-level and two-level modes. Although this converter can realize a wide voltage gain range with the fixed-frequency control, two operating modes imply more sophisticated control and not all the switches endure half of the input voltage under the three-level mode. A fixed-frequency TL LLC converter with auxiliary switches and windings on the secondary side is presented in [21]. However, additional windings are added on the secondary side of the transformer and the secondary auxiliary switches cannot realize ZVS turn-on.

Furthermore, some other types of LLC resonant converter, which are suitable for wide input voltage applications are also proposed. Hu *et al*. [22] proposed an LLC resonant converter with two transformers, by operating in four different modes, the

Manuscript received July 17, 2015; revised November 10, 2015; accepted February 2, 2016. Date of publication February 16, 2016; date of current version September 16, 2016. This work was supported by the National Natural Science Foundation of China under Grants 51077112 and 51407155, and by the Natural Science Foundation of Hebei Province under Grants E2015203407 and 13211907D-2. Recommended for publication by Associate Editor C. A. Canesin.

X. Sun, X. Li, B. Wang, and X. Guo are with the Key Lab of Power Electronics for Energy Conservation and Motor Drive of Hebei Province, Department of Electrical Engineering,Yanshan University, Qinhuangdao 066004, China (e-mail: sxf@ysu.edu.cn; 787860416@qq.com; bcwang@ysu.edu.cn; gxq@ysu.edu.cn).

Y. Shen is with the Department of Energy Technology, Aalborg University, Aalborg 9220, Denmark (e-mail: yaf@et.aau.dk).

Color versions of one or more of the figures in this paper are available online at http://ieeexplore.ieee.org.

Digital Object Identifier 10.1109/TPEL.2016.2530748

normalized dc voltage gain range can be as wide as four times the minimum input voltage, but the parameter design procedure is too complicated. A cascaded two-stage LLC converter consisting of an interleaved boost converter and an FB LLC converter for plug-in electric vehicles is discussed in [23]. Similarly, in [24], a cascaded two-stage LLC converter consisting of a boost circuit and an HB LLC circuit is introduced for fuel cell application, which can help the LLC converter to operate at a nearly constant resonant frequency over a wide input voltage range. But the boost stage operates in the hard-switching manner, which increases the switching loss and hinders the improvement of efficiency. In [14], by integrating a two-phase interleaved boost converter with an FB LLC converter, an interleaved boost-integrated LLC resonant converter with fixed-frequency PWM control is proposed. Although the regulated gain range and the input current ripple can be extended and reduced, respectively, the number of magnetic components is increased, and the two boost inductors may have the problem of uneven currents.

The topology in [25] is a dual-bridge (DB) pulsewidth-modulated (PWM) dc/dc converter with ZVS, which can operate over a wide voltage range and have a smaller output filter inductor. Unlike the phase-shift FB PWM converter, this converter can achieve ZVS at a fixed switching frequency with no need for phase-shift control. However, the ZVS is realized by utilizing the leakage inductance of the transformer. Therefore, the ZVS range is limited and depends on the load condition. Although the ZVS load range can be widened by increasing the leakage inductance of the transformer or adding an external inductor in series with the transformer primary winding, it results in high loss of volt-seconds, thereby requiring the transformer turns ratio to be compromised [26]. Moreover, the secondary diodes have the problem of reverse recovery.

This paper proposes a fixed-frequency DB LLC resonant converter for wide input voltage range applications. The topology can be seen as a combination of the HB LLC converter and the FB LLC converter. The output voltage is regulated by controlling the percentage of operating time of the FB and HB during a switching circle. This converter employs the fixed-frequency PWM control, and the switching frequency equals to the resonant frequency, which facilitates the design of magnetic elements. Unlike traditional PFM-controlled LLC resonant converters, the voltage gain range is independent of the quality factor Q. Moreover, the magnetizing inductor has little influence on the voltage gain, which means that the parameter design process can be simplified, and the magnetizing inductor can be designed as large as possible to reduce the conduction loss. In addition, all main switches and rectifier diodes are softly switched over the full load range, which significantly decreases the switching loss and the reverse recovery loss.

This paper is thus organized with Section II introducing the topology and modulation schedule of the proposed DB LLC resonant converter and Section III concentrating on the operating modes in the converter. Performances of the converters are then analyzed in Section IV, before experimental results are presented in Sections V. Conclusions drawn are finally presented in Section VI.

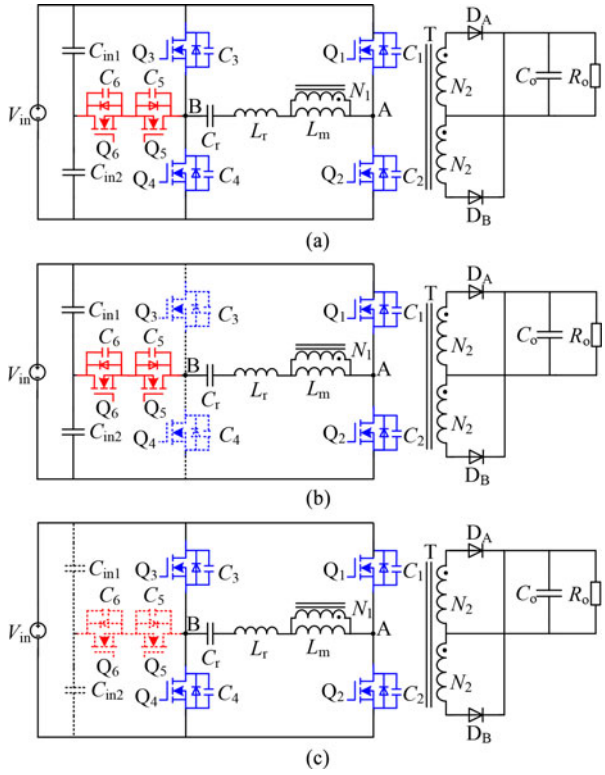

Fig. 1. (a) Proposed DB LLC resonant converter. (b) Equivalent circuit when the proposed DB LLC resonant converter operates in the HB mode. (c) Equivalent circuit when the proposed DB LLC resonant converter operates in the FB mode.

II. Topology and Modulation of the Proposed DB LLC Converter

A. Topology Description

Fig. 1(a) shows the circuit diagram of the proposed converter. The divided capacitors $C_{\rm in1}, C_{\rm in2}$ and output filter C_o are assumed to be large enough, and thus, they are regarded as three constant-voltage sources. C_1-C_6 are the junction capacitors of power switches, and we assume $C_1 = C_2 = C_3 = C_4 = C_5 = C_6 = C_{\rm oss}$. The three-element resonant tank is composed of L_r, C_r, and L_m. The center-tapped transformer with a turns ratio of $N_1 : N_2 : N_2 = n : 1 : 1$. Switches Q_1, Q_2, Q_5, and Q_6 and capacitors $C_{\rm in1}, C_{\rm in2}$ constitute an HB, as shown in Fig. 1(b), whereas switches Q_1, Q_2, Q_3, and Q_4 compose an FB, as shown in Fig. 1(c). Therefore, this converter can be seen as a combination of the HB and FB circuits. When the converter operates in the HB mode, switches Q_5 and Q_6 are on and Q_3 and Q_4 are kept off all the time. When the converter enters into the FB mode, switches Q_5 and Q_6 are kept off always. The *LC* resonant frequency is denoted as $f_r = 1/(2\pi\sqrt{L_r C_r})$.

B. Modulation Schedule

Fixed-frequency PWM control is adopted for the DB LLC resonant converter, and the switching frequency f_s equals to the resonant frequency f_r. Fig. 2 shows the operating waveforms of the proposed converter. Switches Q_1 and Q_2 are operated with

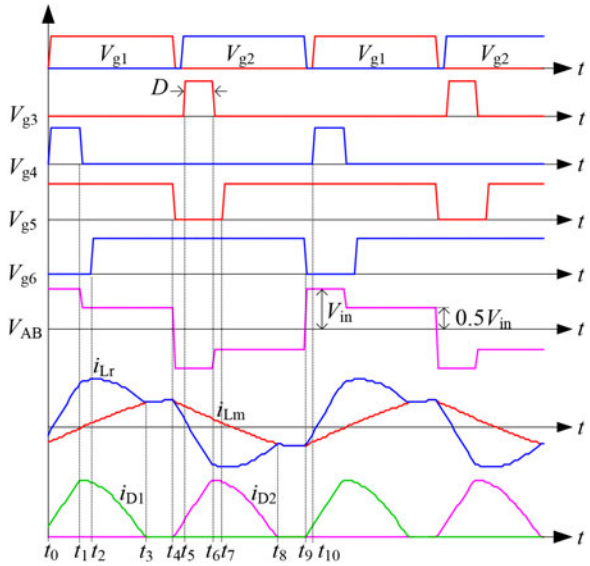

Fig. 2. Key operating waveforms of the DB LLC resonant converter.

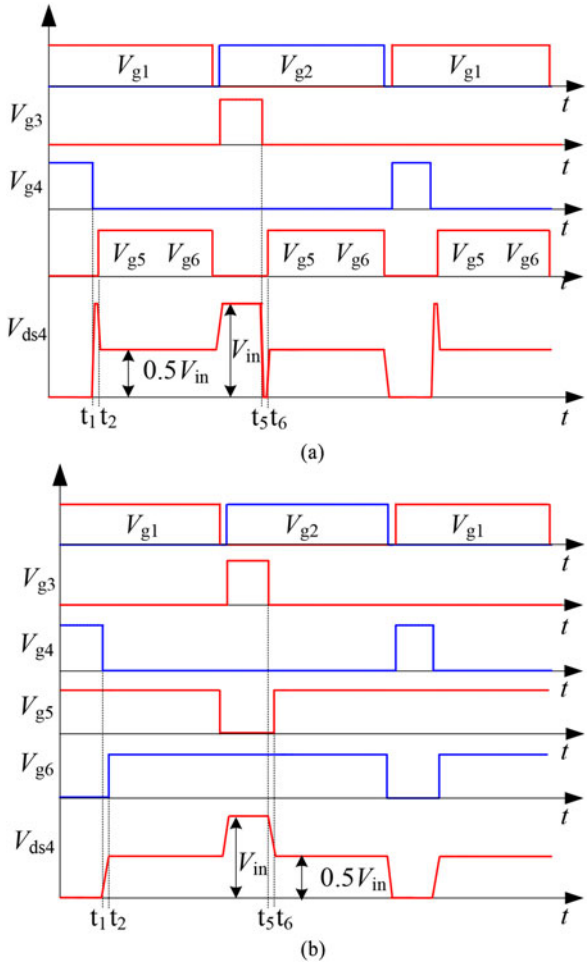

Fig. 3. Two different modulation schedules with Q_5 and Q_6 being driven (a) synchronously and (b) 180° out of phase with each other.

the fixed 50% duty ratio. Switches Q_3 and Q_5 are turned on alternatively, and switches Q_4 and Q_6 are turned on alternatively. The duty ratio of Q_3 and Q_4 is D and that of Q_5 and Q_6 is $1-D$. The variation range of duty ratio D is 0–0.5. In this case, the variation of the input voltage is $V_{\max}:V_{\min}=2:1$. When the input voltage is at its minimum value $V_{\min}$, the duty ratio of Q_3 and Q_4 is 50% and that of Q_5 and Q_6 is 50% as well. Then the converter operates like an FB LLC converter with 50% duty ratio. When the input voltage reaches its maximum value $V_{\max}$, the duty ratio of Q_3 and Q_4 is 0, whereas the duty ratio of Q_5 and Q_6 is 1–0% = 100%. In this case, the proposed DB LLC converter operates the same as an HB LLC converter with 50% duty ratio. When the input voltage changes between $V_{\min}$ and $V_{\max}$, the duty ratio of Q_3 and Q_4 changes between 50% and 0% and the duty ratio of Q_5 and Q_6 is from 50% to 100%.

According to Fig. 2, it can be seen that switches Q_5 and Q_6 together play the role of a bidirectional switch. Theoretically, for control brevity, the modulation schedule can be chosen as Fig. 3(a) where Q_5 and Q_6 are driven synchronously. However, the switching frequency of Q_5 and Q_6 in this case is twice as high as that of other devices, and this is not beneficial to the ZVS realization of Q_5 and Q_6. Meanwhile, the drain–source voltages of switches Q_3 and Q_4 are different in Fig. 3(a) and (b). For example, a voltage spike appears when the drain–source voltage of Q_4, i.e., V_{ds4}, changes from 0 to $V_{\mathrm{in}}/2$ during the time interval t_1–t_2 if Q_5 and Q_6 are driven synchronously [see Fig. 3(a)], whereas it is free of ringing if Q_5 and Q_6 are driven 180° out of phase with each other, as shown in Fig. 3(b).

The reason for this phenomenon is explained in the following. During the time interval t_1–t_2 in Fig. 3(b), switch Q_5 is conducting, the resonant current i_{L_r} discharges C_6, and V_{ds4} increases until the body diode of Q_6 turns on, at the same time V_{ds4} is clamped to $V_{\mathrm{in}}/2$. However, since both Q_5 and Q_6 are turned off, C_6 and C_5 are always being discharged and charged, respectively, during the whole interval t_1–t_2 in Fig. 3(a). Correspondingly, V_{ds4} keeps on increasing to the input voltage, until the driving signal of switch Q_5 comes and V_{ds4} is clamped to $V_{\mathrm{in}}/2$. It is also can be seen that when Q_5 and Q_6 are driven synchronous, Q_3 and Q_4 endure a larger dv/dt, and Q_5 and Q_6 operate in a hard-switching manner.

Besides, when employing the modulation schedule shown in Fig. 3(b), ZVS for switches Q_5 and Q_6 is realized automatically. During the transition from Q_4 off to Q_6 on (t_1–t_2), the drain–source voltage of Q_6 goes to approximately zero and the body diode of Q_6 conducts. Though the gate control signal of Q_6 may have already arrived before the body diode of Q_6 conducts, Q_6 will not conduct until the drain–source voltage of Q_6 decreases to zero, and ZVS is realized automatically. The switch Q_5 experiences the similar processes.

III. Operating Principle of the Proposed DB LLC Converter

As shown in Fig. 2, the operating process of the proposed DB LLC resonant converter can be divided into two half-cycles:

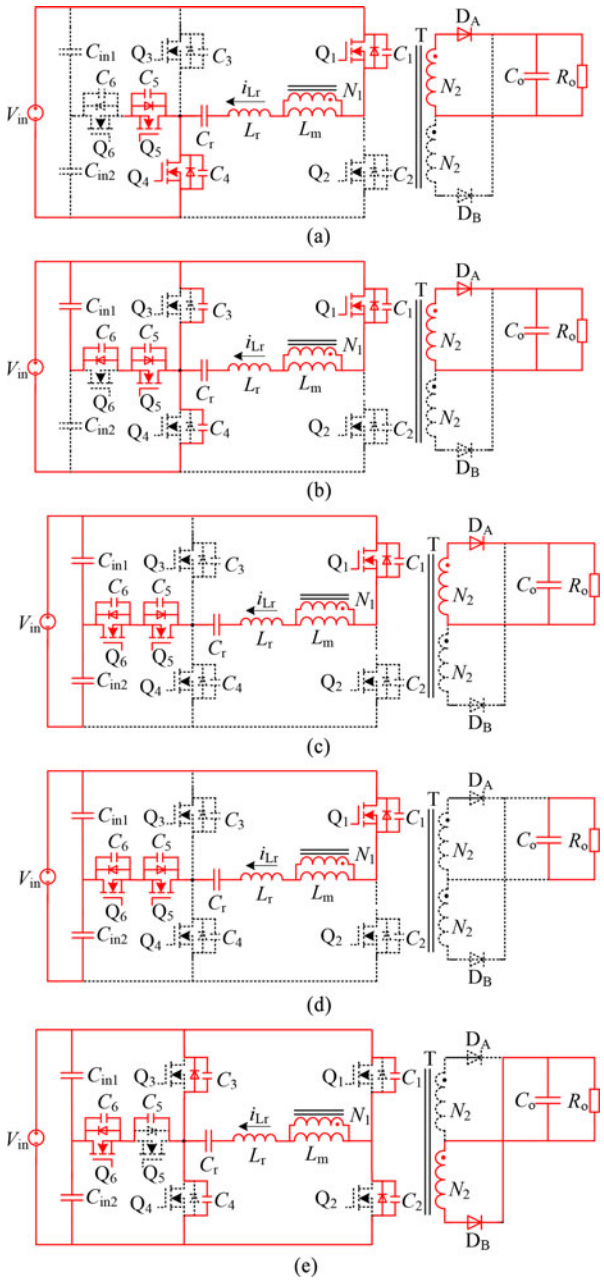

Fig. 4. Operating modes of the DB LLC converter with fixed-frequency PWM control. (a) Stage 1 [t_0, t_1]. (b) Stage 2 [t_1, t_2]. (c) Stage 3 [t_2, t_3]. (d) Stage 4 [t_3, t_4]. (e) Stage 5 [t_4, t_5].

t_0–t_5 and t_5–t_{10}. And there are five operating steps during half a switching cycle. Since two half-cycles are symmetric, only t_0–t_5 is introduced and the corresponding equivalent circuits are shown in Fig. 4.

Stage 1 [t_0, t_1] [see Fig. 4*(a)]:* Q_5 has been conducting before this stage, Q_1 and Q_4 are turned on at t_0. During this time interval, the converter operates in the FB mode, and the resonant tank voltage $V_{\rm AB}$ equals the input voltage $V_{\rm in}$. The primary resonant current i_{L_r} is sinusoidal due to the resonance between L_r and C_r. Because the magnetizing inductor voltage V_{L_m} is clamped at nV_o, where n is the turn ratio and V_o is the output voltage, the magnetizing current i_{L_m} is increasing linearly. The rectifier diode D_A is conducting, and the difference between i_{L_r} and i_{L_m} is transferred to the output stage.

To simplify the analysis, normalized variables are used in the equations and expressions throughout the paper. Define the voltage, current, and frequency bases as

$$\begin{cases} V_{\rm BASE} = V_{\rm in} \\ I_{\rm BASE} = \frac{V_{\rm in}}{Z_r} \\ f_{\rm BASE} = f_r \end{cases} \tag{1}$$

where the characteristic impedance $Z_r = \sqrt{L_r/C_r}$.

Therefore, the normalized currents i_{L_r}, i_{L_m}, and the voltage across the resonant capacitor V_{C_r} can be expressed as

$$\begin{cases} i^*_{L_r}(\theta) = i^*_{L_r}(0)\cos\theta + k_1\sin\theta \\ V^*_{C_r}(\theta) = 1 - M - k_1\cos\theta + i^*_{L_r}(0)\sin\theta \\ i^*_{L_m}(\theta) = i^*_{L_r}(0) + M\theta/m \end{cases} \tag{2}$$

where the voltage gain $M = nV_o/V_{\rm in}$, the inductor ratio $m = L_m/L_r$, $\theta = \omega_r t$, $\omega_r = 1/\sqrt{L_r C_r}$, $k_1 = 1 - M - V^*_{C_r}(0)$, and $\theta_0 = \omega_r t_0 = 0$.

Stage 2 [t_1, t_2] [see Fig. 4*(b)]:* At t_1, Q_4 is turned off. During this time interval, the primary resonant current i_{L_r} begins to charge C_4 and discharge C_3 and C_6. The drain–source voltage of Q_5 is zero because it is kept conducting during this period. When the drain–source voltage of Q_4 increases to $V_{\rm in}/2$, the drain–source voltage of Q_6 decreases to zero and ZVS turn-ON of Q_6 can be achieved until the driving signal comes. The resonant tank voltage $V_{\rm AB}$ during this time changes from $V_{\rm in}$ to $V_{\rm in}/2$.

Stage 3 [t_2, t_3] [see Fig. 4*(c)]:* Q_6 is turned on under ZVS at t_2, and Q_1, Q_5, and D_A are still in on-state. During this time interval, the converter operates in HB mode and the resonant tank voltage $V_{\rm AB}$ equals to $V_{\rm in}/2$. The magnetizing voltage V_{L_m} is still clamped to the output voltage, and the magnetizing current i_{L_m} keeps on linearly increasing. And the operation of this stage is similar to stage 1, only the amplitudes of voltage across the resonant tank are different. The normalized currents i_{L_r}, i_{L_m}, and the voltage across the resonant capacitor V_{C_r} can be expressed as

$$\begin{cases} i^*_{L_r}(\theta) = i^*_{L_r}(\theta_1)\cos(\theta-\theta_1) \\ \quad + \left(1/2 - M - V^*_{C_r}(\theta_1)\right)\sin(\theta-\theta_1) \\ V^*_{C_r}(\theta) = 1/2 - M - \left(1/2 - M - V^*_{C_r}(\theta_1)\right) \\ \quad \cos(\theta-\theta_1) + i^*_{L_r}(\theta_1)\sin(\theta-\theta_1) \\ i^*_{L_m}(\theta) = i^*_{L_r}(\theta_1) + M(\theta-\theta_1)/m \end{cases} \tag{3}$$

where $\theta_1 = \omega_r t_1 = D_0\pi$ and $D_0 = 2D$.

Stage 4 [t_3, t_4] [see Fig. 4*(d)]:* During this stage, the converter is still operating in HB mode and the resonant current i_{L_r} equals to magnetizing current i_{L_m} and the magnetizing inductor L_m starts to resonate together with L_r and C_r instead of being clamped. The rectifier diode D_A is turned off, with ZCS avoiding the reverse recovery. Since output is separated from primary, the power to the load is only supplied by the output capacitor C_o. And the resonant current i_{L_m} during this stage can be called circulating current [15], which is not beneficial for efficiency

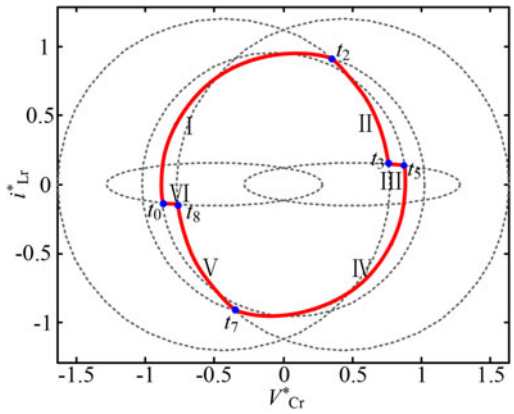

Fig. 5. Steady-state trajectory.

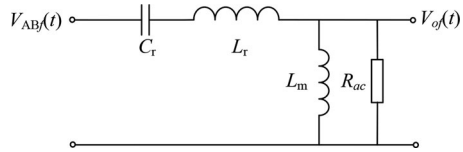

Fig. 6. AC-equivalent circuit for FHA analysis.

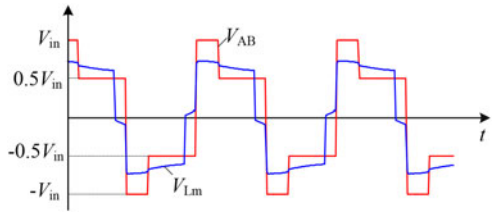

Fig. 7. Voltage waveforms across the resonant tank and magnetizing inductance.

improving. And voltages and currents during this mode can be described as follows:

$$\begin{cases} i^*_{L_r}(\theta) = i^*_{L_r}(\theta_3)\cos\left(k_2(\theta-\theta_3)\right) \\ \quad + \left(1/2V^*_{C_r}(\theta_3)\right) k_2 \sin\left(k_2(\theta-\theta_3)\right) \\ V^*_{C_r}(\theta) = 1/2 - \left(1/2 - V^*_{C_r}(\theta_3)\right)\cos\left(k_2(\theta-\theta_3)\right) \\ \quad + k_2^{-1} i^*_{L_r}(\theta_3)\sin\left(k_2(\theta-\theta_3)\right) \\ i^*_{L_m}(\theta) = i^*_{L_r}(\theta) \end{cases} \quad (4)$$

where $k_2 = 1/\sqrt{1+m}$, $\theta_3 = \omega_r t_3$, and $\theta_4 = \omega_r t_4 = \pi$.

Stage 5 [t_4, t_5] [see Fig. 4*(e)]:* At the moment of t_5, Q_1 and Q_5 are turned off. During this dead-time interval, C_1, C_4, and C_5 are charged by the resonant current and their drain–source voltages increase. Correspondingly, C_2 and C_3 are discharged until their body diodes conduct and ZVS turn on for switches Q_2 and Q_3 can be achieved subsequently.

Fig. 5 shows the trajectory loci when mapping the normalized resonant current and the resonant voltage to the state plane. Ignoring the dead time, the start time of each stage is shown in Fig. 5 and the six different operating steps of the converter are denoted by mode I through VI. The circle centers of mode I through VI are $(1-M, 0)$, $(0.5-M, 0)$, $(0.5, 0)$, $(M-1, 0)$, $(M-0.5, 0)$, and $(-0.5, 0)$. Modes I and IV represent the stages when converter operating in the FB mode, and modes II and V represent the stages when converter operating in the HB mode. The two partial ellipse trajectories of modes III and VI represent the stages when the magnetizing inductor L_m participates in the resonance.

IV. Converter Performance Analysis

A. DC Voltage Gain

The proposed DB LLC converter adopts the fixed-frequency PWM control and the switching frequency equals to the resonant frequency. According to [27], the voltage gain of the converter can be calculated by using the fundamental harmonic approximation (FHA).

Based on FHA, the ac-equivalent circuit for the converter is derived, as shown in Fig. 6. The ac-equivalent load resistance $R_{\rm ac}$ can be obtained as

$$R_{\rm ac} = \frac{8n^2 R_o}{\pi^2}. \quad (5)$$

According to Fig. 2, $V_{\rm AB}$ is a periodical function, which can be expressed as

$$V^*_{\rm AB} = \begin{cases} 1, & 0 \le \theta \le 2\pi D \\ 0.5, & 2\pi D \le \theta \le \pi \\ -1, & \pi \le \theta \le \pi + 2\pi D \\ -0.5, & \pi + 2\pi D \le \theta \le 2\pi. \end{cases} \quad (6)$$

Using the Fourier decomposition, the normalized fundamental component of $V_{\rm AB}(t)$ is given by

$$\begin{cases} V^*_{ABf}(\theta) = \dfrac{\sqrt{10 - 6\cos 2\pi D}}{\pi}\sin(\theta+\varphi) \\ \varphi = \arctan\left(\dfrac{3-\cos 2\pi D}{\sin 2\pi D}\right). \end{cases} \quad (7)$$

$V_{\rm of}(t)$ denotes the fundamental component of the output voltage referred to the primary side, which is given in (8), and the voltage gain M is given in (9)

$$V^*_{\rm of}(\theta) = \frac{4}{\pi} M \sin\theta \quad (8)$$

$$M = \frac{nV_o}{V_{\rm in}} = \sqrt{10 - 6\cos 2\pi D}/4. \quad (9)$$

However, FHA considers the current and voltage waveforms as pure sinusoids at the fundamental frequency and neglects high-order harmonics. Therefore, the accuracy drops when the current/voltage waveforms become more nonsinusoidal [28]. Meanwhile, the voltage across the magnetizing inductance is considered as a square wave, but in reality, the voltage of the magnetizing inductance V_{L_m} distorts significantly, as shown in Fig. 7. Thus, it is difficult to obtain its fundamental component. As a result, FHA cannot predict the gain characteristics of the DB LLC converter accurately, which means (9) is inappropriate. Therefore, time-domain analysis is conducted in order to get more precise gain characteristics [14].

On the basis of odd symmetry, the ending values of i_{L_r}, i_{L_m}, and V_{C_r} should be opposite to their initial values in steady state over a half cycle, i.e.,

$$\begin{cases} V_{C_r}^*(\theta_0) = -V_{C_r}^*(\theta_4) \\ i_{L_r}^*(\theta_0) = -i_{L_r}^*(\theta_4) \\ i_{L_r}^*(\theta_3) = i_{L_m}^*(\theta_3). \end{cases} \tag{10}$$

Besides, the average value of the difference between resonant current i_{L_r} and magnetizing current i_{L_m} over half a cycle equals the output current. Thus, the output current can be expressed as

$$\frac{1}{\pi}\int_0^{\pi} (i_{L_r}^*(\theta) - i_{L_m}^*(\theta))d\theta = I_o^* = \frac{8MQ}{\pi^2} \tag{11}$$

where the quality factor Q is defined as

$$Q = \frac{\pi^2 Z_r}{8n^2 R_o}. \tag{12}$$

Ignoring the dead time and combining (2)–(4), (10)–(12), we can obtain the steady-state equation set

$$\begin{cases} i_{L_r}^*(0) + \cos\big(k_2(\theta_4-\theta_3)\big)\big[i_{L_r}^*(0)\cos\theta_3 + k_1\sin\theta_3 \\ \quad -\sin\big(\theta_3-\theta_1\big)/2\big] + k_2\sin\big(k_2(\theta_4-\theta_3)\big)\big[M \\ \quad -\cos\big(\theta_3-\theta_1\big)/2 + k_1\cos\theta_3 - i_{L_r}^*(0)\sin\theta_3\big] = 0 \\ 1/2 + V_{C_r}^*(0) - \cos\big(k_2(\theta_4-\theta_3)\big)\big[M - \cos\big(\theta_3-\theta_1\big)/2 \\ \quad +k_1\cos\theta_3 - i_{L_r}^*(0)\sin\theta_3\big] + k_2^{-1}\sin\big(k_2(\theta_4-\theta_3)\big) \\ \quad \big[i_{L_r}^*(0)\cos\theta_3 + k_1\sin\theta_3 - \sin\big(\theta_3-\theta_1\big)/2\big] = 0 \\ i_{L_r}^*(0)\big(\cos\theta_3 - 1\big) + k_1\sin\theta_3 - \sin\big(\theta_3-\theta_1\big)/2 = M\theta_3/m \\ k_1\big(1-\cos\theta_3\big) + \big(\cos\big(\theta_3-\theta_1\big)-1\big)/2 + i_{L_r}^*(0) \\ \quad \big(\sin\theta_3 - \theta_3\big) = M(\theta_3^2/2m + 8Q/\pi). \end{cases} \tag{13}$$

By numerically solving (13), the characteristics of dc voltage gain M versus duty cycle D_0 ($D_0 = 2D$) can be depicted for different parameters (including the quality factor Q and the inductor ratio m), as shown in Fig. 8. Fig. 8(a) plots the curves of dc voltage gain M versus duty cycle D_0 for different Q at $m = 4$ and different m at $Q = 0.3$. In order to verify the accuracy of numerical calculation, the simulation results with the same parameters are presented in Fig. 8(a) as well. A full circuit of the DB LLC resonant converter with open-loop control is built and simulated with PSIM 9.03. The input voltage of the circuit is 200 V, and the transformer turns ratio is 5:1:1. The resonant tank parameters are shown as follows: $L_r = 11.6\ \mu$H and $C_r = 218.3$ nF. The switching frequency f_s is 100 kHz, which is equal to the LC resonant frequency f_r. It can be seen that the numerical calculation results show a good agreement with the simulation results. The dc voltage gain M remains unchanged when the duty cycle D_0 is 0 and 1, which means the voltage gain range of the DB LLC resonant converter is independent of the quality factor Q. Unlike the traditional PFM-controlled LLC resonant converter, there is no need to consider the influence of quality factor Q on the voltage gain range. Meanwhile, the inductor ratio m has little influence on the gain characteristics, as illustrated in Fig. 8(b), which is also quite different from the conventional LLC converter with PFM control.

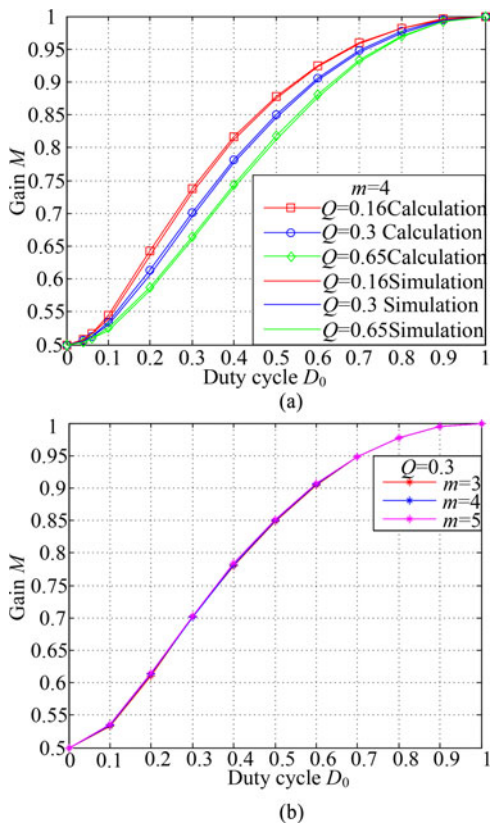

Fig. 8. Gain curves for the DB LLC resonant converter. (a) calculated and simulated results with different quality factor Q; (b) calculated results with different inductor ratio m.

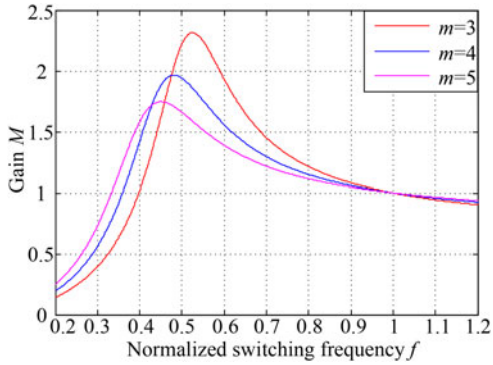

Fig. 9. Gain curves for conventional PFM-controlled FB LLC resonant converter with different inductor ratios.

Fig. 9 shows the curves of dc voltage gain M versus normalized switching frequency f ($f = f_s/f_r$) with different m. It can be seen that for the conventional PFM-controlled LLC converter, the inductor ratio m has a significant impact on the voltage gain: the voltage gain decreases as the inductor ratio m increases. For a wide input voltage range, in order to achieve high gain, the inductor ratio has to be set to a small value, which leads to high magnetizing current and then increasing the conduction

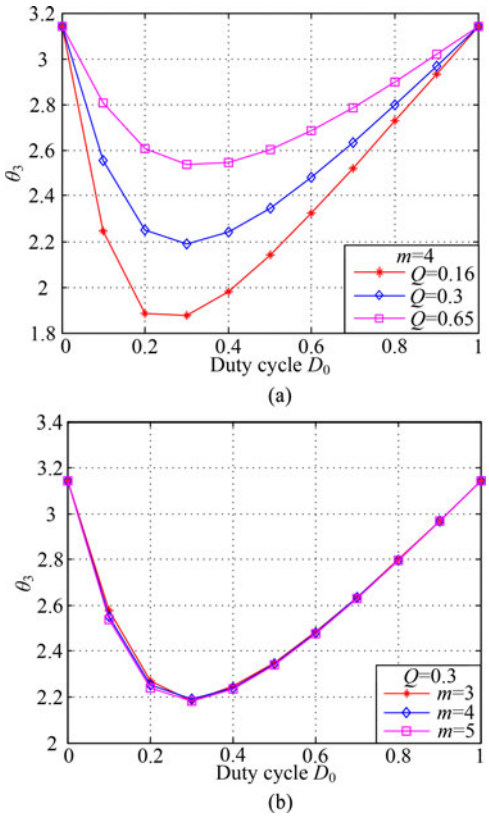

Fig. 10. Curves of θ_3 versus duty ratio D_0 with different (a) quality factor Q and (b) inductor ratio m.

loss [22]. It is very challenging to design parameters within a wide input voltage range while maintaining high efficiency. For the proposed DB fixed-frequency PWM-controlled LLC converter, however, because m has little effect on the voltage gain, the inductor ratio m can be chosen as large as possible, which is beneficial to parameter design and efficiency improving.

B. Parameter Design and ZVS Analysis

By numerically solving (13), the curves for θ_3 versus duty cycle D_0 for different quality factor Q or different inductor ratio m can be obtained, where θ_3 represents the moment that resonant current i_{L_r} begins to equal the magnetizing current i_{L_m}. As seen from Fig. 10(b), m has little influence on θ_3. However, in Fig. 10(a), θ_3 rises with the increase of Q, which means the time interval of stage 4 can be shorter when Q is larger. This is good for reducing the conduction loss and improving efficiency.

The maximum (peak) resonant capacitor voltage ($V_{C_{\rm rp}}$) is reached when the resonant current equals zero. An expression for $V_{C_{\rm rp}}$ can be found by substituting $i^*_{Lr}(\theta) = 0$ into (2)

$$V^*_{C_{\rm rp}} = \left| \begin{array}{l} 1 - M - k_1 \cos(\arctan(-i^*_{L_r}(0)/k_1)) \\ +i^*_{L_r}(0) \sin(\arctan(-i^*_{L_r}(0)/k_1)) \end{array} \right|. \quad (14)$$

By substituting the known value of M, k_1, $i^*_{L_r}(0)$ and $V^*_{C_r}(0)$ into (14), the peak capacitor voltage can be obtained. Fig. 11 shows that the curves of $V^*_{C_{\rm rp}}$ versus duty cycle D_0 for a different quality factor Q can be obtained. From Fig. 11, we can see that the peak capacitor voltage of resonant capacitor $V_{C_{\rm rp}}$ increases as Q gets larger. In order to reduce the circulating current loss, a larger Q should be selected. However, the resonant capacitor withstands excessive voltage stress when the quality factor Q is overlarge. Thus, a tradeoff must be made when selecting the quality factor Q. A moderate quality factor Q of 0.65 under full-load conditions is selected in this paper.

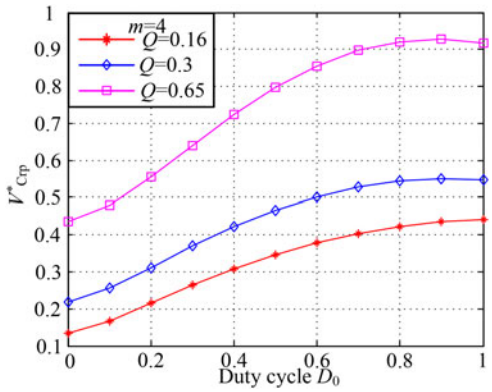

Fig. 11. Curves of calculated $V^*_{C_{\rm rp}}$ versus duty ratio D_0 with a different quality factor Q.

TABLE I
COMPARISON OF FOUR CONVERTER TOPOLOGIES

Topologies	FB LLC Converter [29]	Hybrid FB Three-Level LLC [20]	Three-Level Fixed-Frequency LLC Converter [21]	Proposed DB LLC Resonant Converter
Number of switches	4	6	6	6
Number of diodes (with center-tapped rectifier)	2	4	6	2
Number of transformer's secondary windings	2	2	4	2
Flying capacitor	No	Yes	Yes	No
Modulation	PFM	PWM + Phase-shift	Phase-shift	PWM
Gain range	Narrow	Wide	Wide	Wide
Input range	300–400 V	200–400 V	400–650 V	120–240 V
Full-load efficiency	95%	95.1%	87.23%	94.1%
Output Power	48 V/12 A	360 V/4 A	60 V/44.5 A	24 V/20 A

Once Q is decided, the resonant capacitor C_r and resonant inductor L_r can be calculated by the formula of resonant frequency and (12). The magnetizing inductor L_m can be obtained if the inductor ratio m is decided. Since the inductor ratio m has little influence on the voltage gain, it can be chosen as large as possible to reduce the conduction loss. The ZVS is realized by discharging the junction capacitor of MOSFET during the dead time interval. Therefore, the current cannot be too small. Meanwhile, as the m increases, the magnetizing current will get smaller, which does not contribute to the realization of ZVS. Therefore, when selecting the value of m, ZVS should be considered as well.

As aforementioned, switches Q_5 and Q_6 can automatically realize ZVS. Therefore, only switches Q_1–Q_4 need to be taken

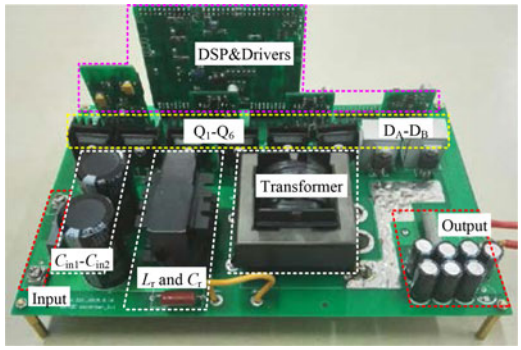

Fig. 12. Laboratory prototype.

TABLE II
COMPONENT LIST

Components	Parameters
Primary switches (Q_1–Q_6)	SPW20N60C3
Secondary rectification switches (D_A – D_B)	IPP045N10N
Transformer turns ratio (N_1:N_2:N_2)	10:2:2
Magnetizing inductance (L_m)	170 μH
Resonant inductance (L_r)	25.3 μH
Resonant capacitor (C_r)	100 nF
Input capacitor(C_{in1}, C_{in2})	220 μF
Output capacitor (C_o)	7 × 680 μF in parallel
Dead time	400 ns

into account. During the commutation process, the drain–source voltage of Q_1 or Q_2 always equals to the input voltage, the drain–source voltage of Q_3 or Q_4 is the input voltage or half of the input voltage. It is already known that the charge of the junction capacitor proportional to its capacitance and the withstanding voltage, and the characteristics of the junction capacitor of Q_1–Q_4 are the same. Thus, it is harder for the switches Q_1 and Q_2 to realize ZVS, which means only Q_1 and Q_2 need to be considered. Since the dead time is short, it is justified to assume that the junction capacitors are charged/discharged with constant current during the ZVS commutation time interval. The minimal commutation current during the dead time interval can be calculated with

$$I_{\min} = \frac{2C_{\text{oss}}V_{\text{in}}}{t_{\text{dead}}}. \tag{15}$$

On the premise of satisfying ZVS, the inductor ratio m is selected as 7 in this research.

C. Comparison of Four Converter Topologies

A comparison of four converter topologies is illustrated in Table I. As mentioned earlier, the conventional FB LLC converter employs PFM control and the inductor ratio m has a considerable effect on voltage gain. The value of m has to be set small when the input voltage range is wide, and small m will lead to higher magnetizing current and higher conduction loss. Therefore, it is difficult to design and optimize the magnetic components when the input voltage range is wide. Compared with the conventional PFM controlled FB LLC converter, the proposed DB LLC resonant converter adopts fixed-frequency

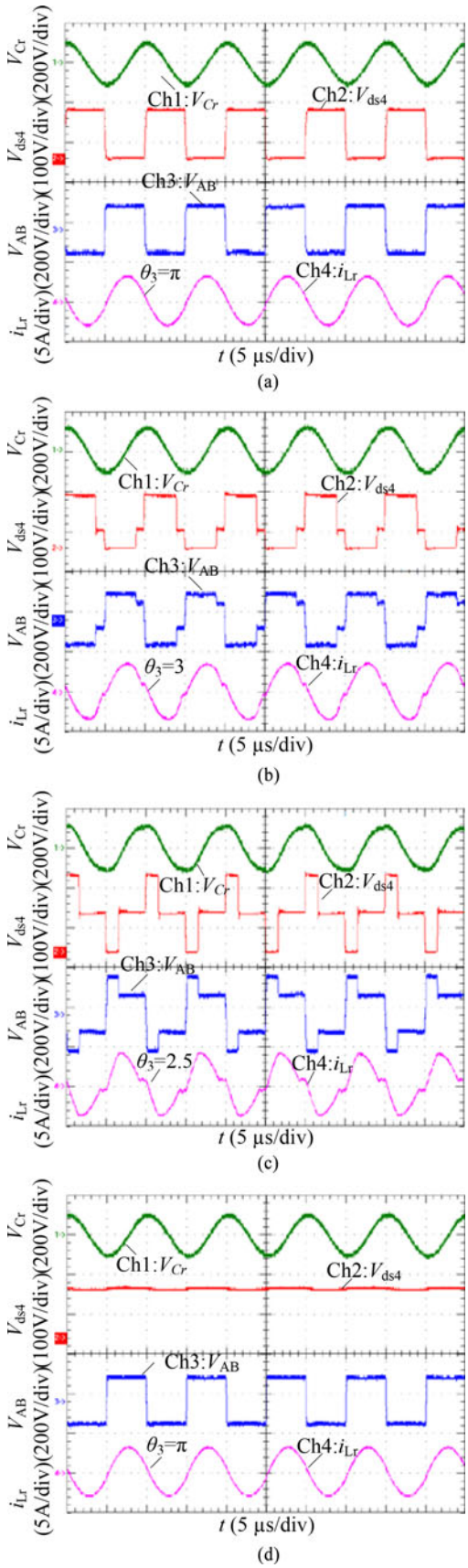

Fig. 13. Measured steady-state voltage and current waveforms at full load with different input voltages. (a) $V_{\text{in}} = 120$ V; (b) $V_{\text{in}} = 130$ V; (c) $V_{\text{in}} = 190$ V; (d) $V_{\text{in}} = 240$ V.

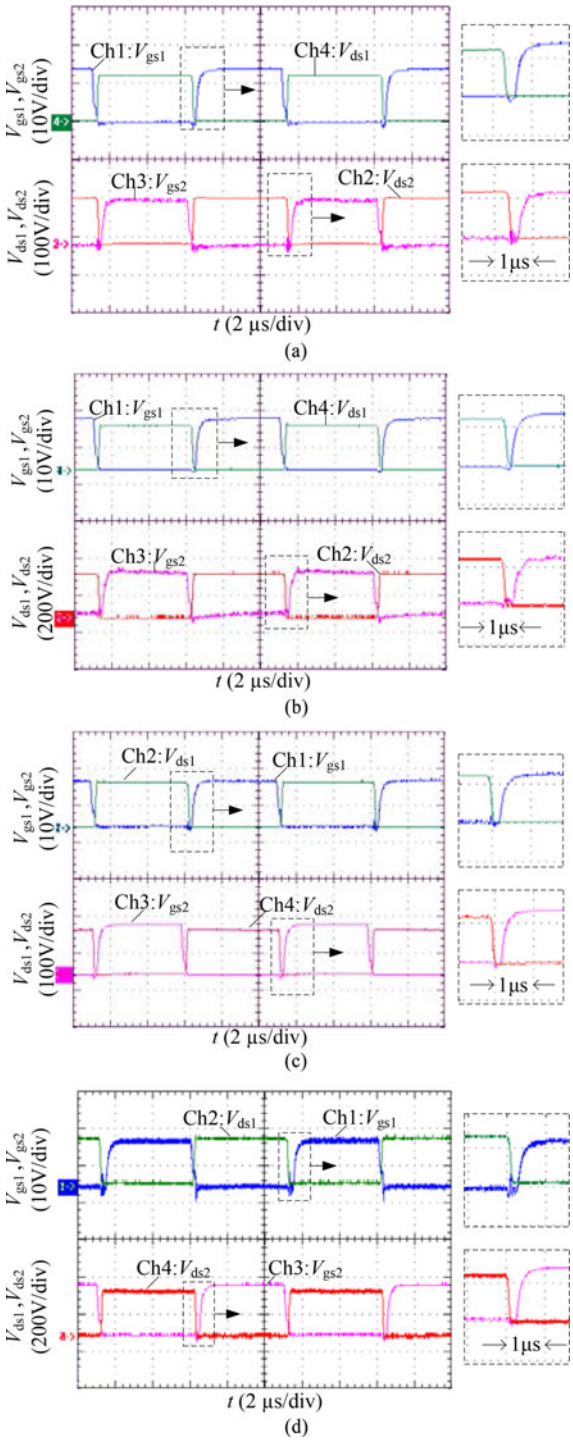

Fig. 14. ZVS waveforms of switches Q_1 and Q_2 with the converter operating at (a) full load with 120 V input, (b) full load with 240 V input, (c) 10% load with 120 V input, and (d) 10% load with 240 V input.

PWM control and the inductor ratio m has little influence on the gain characteristics, which signifies that a larger m can be selected, resulting in lower conduction loss. Therefore, the DB LLC resonant converter is a good candidate for wide input voltage range applications and is very beneficial to parameter design.

As can be seen in Table I, compared with the DB LLC resonant converter, the hybrid FB three-level LLC converter has two more diodes and an extra flying capacitor. Besides, in order to make the converter suitable for wide input voltage applications, PWM and phase-shift control strategies are employed resulting in two operating modes, which is a little complex. Although the converter can operate under three-level mode, not all the switches endure half of the input voltage.

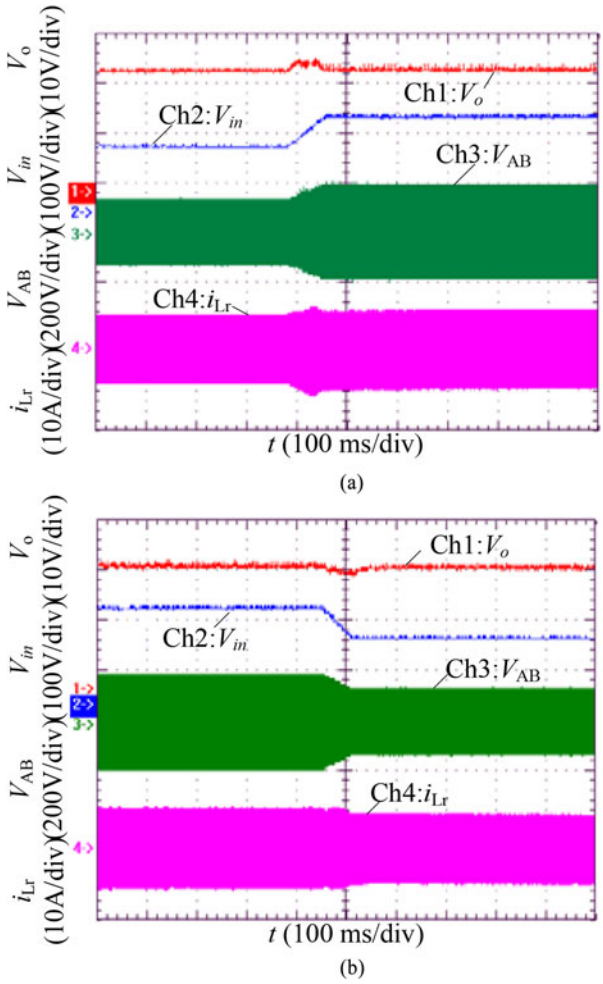

Fig. 15. Experimental results of the DB LLC resonant converter with closed-loop control in response to ramp changes in the input voltage $V_{\rm in}$. (a) Ramp increase of the input voltage $V_{\rm in}$ from 130 to 190 V. (b) Ramp decrease of the input voltage $V_{\rm in}$ from 190 to 130 V.

The three-level LLC converter proposed in [21] applies the phase-shift control between the primary and secondary sides of the transformer to operate at a fixed switching frequency. To improve the performance when the converter is applied to wide input voltage variations, additional windings are added on the secondary side of the transformer, which makes the circuit and the configuration of the transformer more complex. And the flux in the transformer will increase, resulting in higher core losses. In addition, the secondary auxiliary switches can not realize ZVS turn-on, which increases the switching loss.

V. Experimental Results

An experimental prototype was built in order to verify the operating principle and performance of the converter,

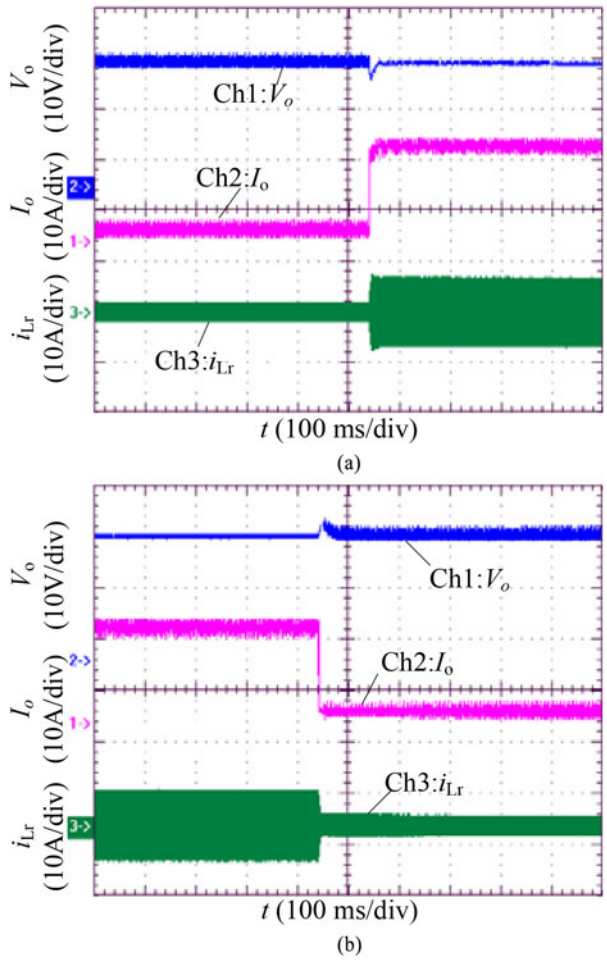

Fig. 16. Experimental results of the DB LLC resonant converter with closed-loop control in response to step changes in the load. (a) Step increase of load from light load to full load. (b) Step increase of load from full load to 10% load.

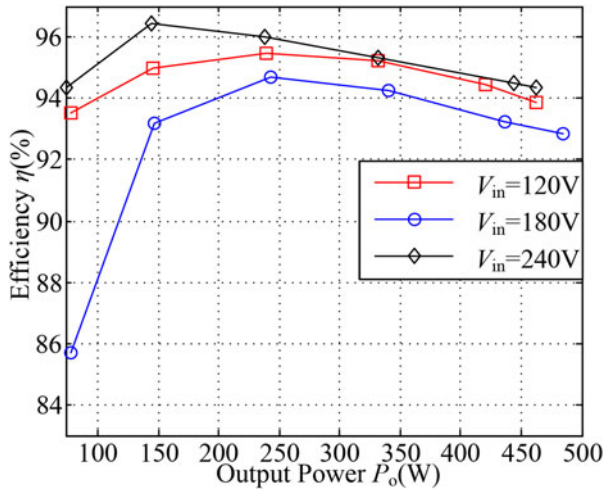

Fig. 17. Measured power stage efficiency of the converter prototype for different input voltages.

as shown in Fig. 12. The specifications of the converter prototype are as follows: input voltage $V_{\rm in} = 120$–240 V, output voltage $V_o = 24$ V, rated output power $P_o = 480$ W, switching frequency $f_s = 100$ kHz, and resonant frequency $f_r = 100$ kHz. Key parameters are listed in Table II.

Fig. 13(a)–(d) shows the waveforms of the voltage of resonant capacitor V_{C_r}, the drain–source voltage $V_{\rm ds4}$ of Q_4, the resonant tank voltage $V_{\rm AB}$, and the resonant current i_{L_r} at full load with different input voltages. Meanwhile, the values of θ_3 under different input voltages are also given. When the input voltage is 120 V, the converter operates in the FB mode, and the resonant tank voltage $V_{\rm AB}$ is a square wave. When the input voltages are 130 and 190 V, the converter operates in the DB mode, the resonant tank voltage $V_{\rm AB}$ is a multilevel step wave and the operating time of the FB decreases as the input voltage increases. When the input voltage is 240 V, the converter operates in the HB mode.

The drain–source voltage and gate driving signal waveforms of Q_1 and Q_2 with 120 and 240 V inputs at 10% load and full load are shown in Fig. 14. The drain–source voltage decreases to zero before the gate driving signal comes, which means that ZVS can be realized under the entire input voltage range and load range.

In order to verify the dynamic performance of the DB LLC resonant converter, Figs. 15 and 16 show the experimental results of the DB resonant converter with closed-loop control in response to ramp changes in the input voltage and step changes in load, respectively. Fig. 15(a) and (b) shows the dynamic responses as input voltage changes. As can be seen, the output voltage V_o can be regulated to 24 V quickly after the input voltage changes, and the overshoot and undershoot for the output voltage V_o are small, which means it can achieve good dynamic performance with respect to input variations under the closed-loop control. In a similar way, Fig. 16(a) and (b) demonstrate that the converter has good performance of the transient response under load changes.

The efficiency of the converter versus output power for different input voltages is shown in Fig. 17. As can be seen, the efficiency is lower when the input voltage is 180 V. This is because when the input voltage is 180 V, the time interval of the resonant current being equal to the magnetizing current is longer, thereby leading to increased conduction loss.

VI. Conclusion

A fixed-frequency-controlled DB LLC resonant converter with a wide input range has been proposed in this paper. In the proposed DB LLC resonant converter, two operating modes (HB and FB modes) are identified and utilized to regulate the output voltage within a wide input voltage range. The modulation strategy, operating principle and characteristics are investigated in depth. Compared with a conventional PFM-controlled LLC converter, the proposed DB LLC resonant converter adopts the fixed-frequency PWM control. The voltage gain range is independent of the quality factor Q and the magnetizing inductance has little impact on the dc voltage gain characteristics. Thus, the process of parameter design can be simplified and also a larger inductor ratio can be chosen to reduce the conduction loss. The structure and control strategy of the DB LLC resonant converter

are simpler compared with conventional fixed-frequency TL LLC resonant converters. The performance of the proposed DB LLC resonant converter is experimentally verified on a 120–240 V input 24 V/20 A output converter prototype. All primary-side switches operate with ZVS and secondary-side diodes turn off with ZCS within wide input voltage and full-load ranges. Also, good dynamic performance with respect to input variations and load changes can be achieved under the closed-loop control. Therefore, the DB LLC resonant converter is a good candidate for wide input voltage applications.

REFERENCES

[1] M. M. Jovanović and B. T. Irving, "On-the-fly topology-morphing control-efficiency optimization method for LLC resonant converters operating in wide input- and/or output-voltage range," *IEEE Trans. Power Electron.*, vol. 31, no. 3, pp. 2596–2608, Mar. 2016.

[2] J. Deng, C. C. Mi, R. Ma, and S. Li, "Design of LLC resonant converters based on operation-mode analysis for level two PHEV battery chargers," *IEEE Trans. Mechatronics*, vol. 20, no. 4, pp. 1595–1606, Aug. 2015.

[3] D. Moon, J. Park, and S. Choi, "New interleaved current-fed resonant converter with significantly reduced high current side output filter for EV and HEV applications," *IEEE Trans. Power Electron.*, vol. 30, no. 8, pp. 4264–4271, Jun. 2015.

[4] F. Musavi, M. Craciun, D. S. Gautam, and W. Eberle, "Control strategies for wide output voltage range LLC resonant DC–DC converters in battery chargers," *IEEE Trans. Veh. Technol.*, vol. 63, no. 3, pp. 1117–1125, Jun. 2014.

[5] C. W. Tsang, M. P. Foster, D. A. Stone, and D. T. Gladwin, "Analysis and design of LLC resonant converters with capacitor-diode clamp current limiting," *IEEE Trans. Power Electron.*, vol. 30, no. 3, pp. 1345–1355, Mar. 2015.

[6] B. Yang, F. C. Lee, A. J. Zhang, and G. Huang, "LLC resonant converter for front end DC/DC conversion," in *Proc. IEEE APEC Expo.*, 2002, vol. 2, pp. 1108–1112.

[7] H. Wang, S. Dusmez, and A. Khaligh, "Maximum efficiency point tracking technique for LLC-based PEV chargers through variable DC link control," *IEEE Trans. Ind. Electron.*, vol. 61, no. 11, pp. 6041–6049, Nov. 2014.

[8] Z. Hu, Y. Qiu, Y. F. Liu, and P. C. Sen, "A control strategy and design method for interleaved LLC converters operating at variable switching frequency," *IEEE Trans. Power Electron.*, vol. 29, no. 8, pp. 4426–4437, Aug. 2014.

[9] K. H. Yi and G. W. Moon, "Novel two-phase interleaved LLC series-resonant converter using a phase of the resonant capacitor," *IEEE Trans. Ind. Electron.*, vol. 56, no. 5, pp. 1815–1819, May 2009.

[10] W. Feng, F. C. Lee, and P. Mattavelli, "Simplified optimal trajectory control (SOTC) for LLC resonant converters," *IEEE Trans. Power Electron.*, vol. 28, no. 5, pp. 2415–2426, May 2013.

[11] G. Yang, D. Patrick, and D. Sadarnac, "Double-phase high-efficiency, wide load rang high-voltage/low-voltage LLC DC/DC converter for electric/hybrid vehicles," *IEEE Trans. Power Electron.*, vol. 30, no. 4, pp. 1876–1886, Apr. 2015.

[12] Z. Guo, D. Sha, and X. Liao, "Hybrid phase-shift-controlled three-level and LLC DC–DC converter with active connection at the secondary side," *IEEE Trans. Power Electron.*, vol. 30, no. 6, pp. 2985–2996, Jun. 2015.

[13] R. Beiranvand, B. Rashidian, M. R. Zolghadri, and S. M. H. Alavi, "Using LLC resonant converter for designing wide-range voltage source," *IEEE Trans. Ind. Electron.*, vol. 58, no. 5, pp. 1746–1756, May 2011.

[14] X. Sun, Y. Shen, Y. Zhu, and X. Guo, "Interleaved boost-integrated LLC resonant converter with fixed-frequency PWM control for renewable energy generation applications," *IEEE Trans. Power Electron.*, vol. 30, no. 8, pp. 4312–4326, Aug. 2015.

[15] Z. G. Liang, R. Guo, G. Y. Wang, and A. Huang, "A new wide input range high efficiency photovoltaic inverter," in *Proc. IEEE Energy Convers. Congr. Expos.*, 2010, pp. 2937–2943.

[16] Y. Gu, Z. Lu, L. Hang, Z. Qian, and G. Huang, "Three-level LLC series resonant DC/DC converter," *IEEE Trans. Power Electron.*, vol. 20, no. 4, pp. 781–789, Jul. 2005.

[17] I. O. Lee and G. W. Moon, "Analysis and design of a three-level LLC series resonant converter for high- and wide-input-voltage applications," *IEEE Trans. Power Electron.*, vol. 27, no. 6, pp. 2966–2979, Jun. 2012.

[18] S. Zong, Q. Luo, C. Li, W. Li, X. He, and S. Su, "Three-level frequency-doubling LLC resonant converter with high step-down ratio for high input voltage applications," in *Proc. IEEE APEC Expo.*, 2014, pp. 14–19.

[19] F. Canales, T. H. Li, and D. Aggeler, "Novel modulation method of a three-level isolated full-bridge LLC resonant DC–DC converter for wide-output voltage application," in *Proc. IEEE PEMC Conf.*, 2012, pp. DS2b.11-1–DS2b.11-7.

[20] K. Jin and X. Ruan, "Hybrid full-bridge three-level LLC resonant converter-a novel DC–DC converter suitable for fuel-cell power system," *IEEE Trans. Ind. Electron.*, vol. 53, no. 5, pp. 1492–1503, Oct. 2006.

[21] F. Canales, P. Babosa, and F. C. Lee, "A wide input voltage and load output variations fixed-frequency ZVS dc/dc LLC resonant converter for high power applications," in *Proc. 37th Ind. Appl. Soc. Annu. Meeting*, Oct. 2002, vol. 4, pp. 2306–2313.

[22] H. Hu, X. Fang, F. Chen, Z. J. Shen, and I. Batarseh, "A modified high-efficiency LLC converter with two transformers for wide input-voltage range applications," *IEEE Trans. Power Electron.*, vol. 28, no. 4, pp. 1946–1960, Apr. 2013.

[23] H. Wang, S. Dusmez, and A. Khaligh, "Design and analysis of a full-bridge LLC-based PEV charger optimized for wide battery voltage range," *IEEE Trans. Veh. Technol.*, vol. 63, no. 4, pp. 1603–1613, Apr. 2014.

[24] J. Y. Lee, Y. S. Jeong, and B. M. Han, "An isolated DC/DC converter using high-frequency unregulated LLC resonant converter for fuel cell applications," *IEEE Trans. Ind. Electron.*, vol. 58, no. 7, pp. 2926–2934, Jul. 2011.

[25] W. Song and B. Lehman, "Dual-bridge DC–DC converter: A new topology characterized with no deadtime operation," *IEEE Trans. Power Electron.*, vol. 19, no. 4, pp. 94–103, Jan. 2004.

[26] R. Ayyanar and N. Mohan, "Novel soft-switching DC–DC converter with full ZVS-range and reduced filter requirement-Part I: Regulated-output applications," *IEEE Trans. Power Electron.*, vol. 16, no. 2, pp. 184–192, Mar. 2001.

[27] T. Y. Jiang, J. M. Zhang, X. K. Wu, K. Sheng, and Y. S. Wang, "A bidirectional three-level LLC resonant converter with PWAM control." *IEEE Trans. Power Electron.*, vol. 31, no. 3, pp. 2213–2225, Mar. 2016.

[28] X. Fang, H. Hu, Z. J. Shen, and I. Batarseh, "Operation mode analysis and peak gain approximation of the LLC resonant converter," *IEEE Trans. Power Electron.*, vol. 27, no. 4, pp. 94–103, Apr. 2012.

[29] R.-L. Lin and C.-W. Lin, "Design criteria for resonant tank of LLC DC–DC resonant converter," in *Proc. IEEE IECON/IECON*, 2010, pp. 427–432.

Xiaofeng Sun (M'11) received the B.S. degree in electrical engineering from Northeast Heavy Machinery Institute, Heilongjiang, China, in 1993, and the M.S. and Ph.D. degrees in power electronics from Yanshan University, Hebei, China, in 1999 and 2005, respectively.

From 2003 to 2007, he was an Associate Professor with Yanshan University, where since 2008 he has been a Professor and also the Director at the Key Laboratory of Power Electronics for Energy Conservation and Motor Drive of Hebei Province. He has authored or coauthored more than 70 transactions and conference papers. His current research interests include dc–dc converters, multiple-input converters, hybrid electric vehicles, microgrids, and power quality control.

Xiaohua Li received the B.S. degree in electrical engineering from Yanshan University, Qinhuangdao, China, in 2013, where she is currently working toward the M.S. degree in power electronics.

Her current research interests include the topology and control of dc–dc converters.

Yanfeng Shen (S'16) received the B.S. and M.S. degrees in electrical engineering and power electronics from Yanshan University, Qinhuangdao, China, in 2012 and 2015, respectively. He is currently working toward the Ph.D. degree in power electronics at Aalborg University, Aalborg, Denmark.

From August 2015 to October 2015, he was an Intern with the ABB Corporate Research Center, Beijing, China. His current research interests include dc–dc converters, inverters, and multi-objective lifecycle optimization of power electronics converters.

Baocheng Wang received the B.S. and M.S. degrees in electrical engineering from Northeast Heavy Machinery Institute, Heilongjiang, China, in 1988 and 1991, respectively, and the Ph.D. degree from Yanshan University, Qinhuangdao, China, in 2008.

Since 2005, he has been a Professor with the Department of Electrical Engineering, Yanshan University. His current research interests include multilevel inverting technology, distributed generation, renewable energy, and fault diagnosis.

Xiaoqiang Guo (SM'14) received the B.S. and Ph.D. degrees in electrical engineering from Yanshan University, Qinhuangdao, China, in 2003 and 2009, respectively.

He has been a Postdoctoral Fellow with the Laboratory for Electrical Drive Applications and Research (LEDAR), Ryerson University, Toronto, ON, Canada. He is currently an Associate professor with the Department of Electrical Engineering, Yanshan University, China. He has authored or coauthored more than 50 technical papers, in addition to nine patents. His current research interests include high-power converters and ac drives, electric vehicle charging station, and renewable energy power conversion systems.